Radial Distribution Functions of Liquid Krypton*

ASHFAQ A. KHAN†
Physics Department, University of Florida, Gainesville, Florida
(Received 6 July 1964)

Radial distribution functions g of liquid krypton have been computed at several values of temperature and density from the Percus-Yevick (PY) and the convolution-hypernetted-chain (CHNC) integral equations using two different interaction potentials [the Lennard-Jones (LJ) and Guggenheim-McGlashan (GM)] between the krypton atoms. The computed g's are compared with the neutron diffraction experimental g's of Clayton and Heaton. From the computed g's, the quantities $i(s)$ which are directly proportional to the experimentally measured quantities (the number of counts/min) have been computed and are compared with the experimental values. Besides this, computations have been done to investigate (i) the behavior of the computed g's with the variation in the range of integration, (ii) the changes in the computed g's with the long-range part of the interaction potential, and (iii) the cause of irregularities in the experimental g's. The g's computed with the CHNC equation and LJ potential with constants due to Beattie *et al.* are in good agreement with the experimental g's except near the critical temperature. The effect on the computed g's of varying the long-range part of pair potential is small. The major cause of the irregularities in the experimental distribution functions is inherent in the experimentally measured intensity curves and not in the truncation error.

I. INTRODUCTION

IN a previous paper[1] we presented the results of computations of radial distribution functions g of argon fluid from the Percus-Yevick[2,3] (PY) and the convolution-hypernetted-chain[4–7] (CHNC) integral equations. In this paper we are presenting the results of similar computations for krypton. The computed g's are compared with the experimental g's from the neutron diffraction experiments by Clayton and Heaton.[8] In the case of argon, the experimental g's were mostly obtained from the x-ray diffraction experiments.[9]

Since our purpose is to reproduce the experimentally determined g from the theoretical computations, it is necessary that we use an interatomic potential for krypton which is as close to the real potential as possible. Several forms of the semiempirical interatomic potentials have been proposed for krypton[10] just as in the case of argon. However, the interatomic potential for krypton is not known as accurately as for argon. We have selected two forms of interaction potentials for the computations of g. They are the Lennard-Jones (LJ) potential with constants determined by Beattie *et al.*[11] and the Guggenheim-McGlashan[12] (GM) potential which has been constructed from the GM potential for argon[13] using the correspondence relation with critical constants. In selecting the values of constants for the LJ potential, we have depended on our experience with argon where we found that the LJ potential used for argon was not sufficiently deep. Several sets of values[14] for the constants of the LJ potential for krypton have been proposed by different authors on the basis of their analysis of the data obtained from the transport and crystal properties of krypton. The set due to Beattie *et al.* is the best compromise in the sense that it is closest to all the other sets due to other authors mentioned in Ref. 14.

The integral equations have been solved for different ranges in order to study the effect on the distribution function and also on the computed thermodynamic quantities. We have also studied the effect of varying the long-range part of the GM potential by giving different values to λ [see Eq. (A4)] on the distribution function and the thermodynamic quantities.

In Sec. II we have briefly discussed the integral equations. In Sec. III we have described the computed distribution and intensity functions, their comparisons with the experimental curves, the effect of changing the range of integration, and the variation of the long-range part of the pair potential on the distribution function. The results of computation and discussion about the irregularities in the experimental g's, and the final conclusions, are given in Sec. IV. The potential functions are given in the Appendix.

* This research was supported in part by funds from the U. S. National Science Foundation and the National Aeronautics and Space Administration.

† Present address: Physics Department, University of Karachi, Karachi, Pakistan.

[1] A. A. Khan, Phys. Rev. **134**, A367 (1964).

[2] J. K. Percus and G. J. Yevick, Phys. Rev. **110**, 1 (1958).

[3] J. K. Percus, Phys. Rev. Letters **8**, 462 (1962).

[4] J. M. J. Van Leeuwen, J. Groeneveld, and J. DeBoer, Physica **25**, 792 (1959).

[5] E. Meeron, J. Math. Phys. **1**, 192 (1960).

[6] T. Morita and K. Hiroike, Progr. Theoret. Phys. (Kyoto) **23**, 1003 (1960).

[7] M. S. Green, Technical Report, Hughes Aircraft Corporation (unpublished).

[8] G. T. Clayton and L. Heaton, Phys. Rev. **121**, 649 (1961).

[9] A. Eisenstein and N. S. Gingrich, Phys. Rev. **62**, 261 (1942).

[10] J. O. Hirschfelder, C. F. Curtiss, and R. B. Bird, *Molecular Theory of Gases and Liquids* (John Wiley & Sons, Inc., New York, 1954).

[11] J. A. Beattie, R. J. Barriault, and J. S. Brierley, J. Chem. Phys. **20**, 1613 (1952).

[12] E. A. Guggenheim and M. L. McGlashan, Mol. Phys. **3**, 563, 1060 (1960). The parts of the potential function not given by Guggenheim and McGlashan were constructed by us.

[13] E. A. Guggenheim and M. L. McGlashan, Proc. Phys. Soc. (London) **225**, 456 (1960).

[14] E. Whallay and W. G. Schneider, J. Chem. Phys. **23**, 1644 (1955); E. A. Mason, J. Chem. Phys. **32**, 1832 (1960); D. D. Konowalow and J. O. Hirschfelder, Phys. Fluids **4**, 629 (1961).

II. THE INTEGRAL EQUATIONS

The pair of equations[15]

$$g(r)=e^{-\beta\phi(r)+N(r)+E(r)} \tag{2.1}$$

and

$$\tilde{N}(k')=n[\tilde{G}(k')]^2/\{1+n[\tilde{G}(k')]\} \tag{2.2}$$

give $g(r)$ exactly. In these equations $\phi(r)$ is the pair potential, $N(r)$ and $E(r)$ are the contributions due to nodal and elementary diagrams[16] respectively, $\tilde{N}(k')$ is the Fourier transform of $N(r)$, $\tilde{G}(k')$ is the Fourier transform of $G(r)$, which is the correlation function $(g(r)-1)$, n is the macroscopic density (number of particles per unit volume) and β is equal to $1/kT$. The above pair of equations can be solved if we know another relation between $N(r)$ and $E(r)$. We write $E(r)$ in terms of $S(r)$ (where $S(r)$ is the contribution due to simple diagrams[16] and is equal to the sum of the nodal and elementary diagrams),[1] and obtain

$$E(r)=Z\left[\frac{S^2}{2!}+\frac{S^3}{3!}+\cdots\right], \tag{2.3}$$

where Z is an unknown function of r, β_ϕ, and density such that Eq. (2.3) holds. The advantage of introducing Z is to regard it as a parameter for the purpose of obtaining approximate integral equations, for when we set Z equal to zero, Eq. (2.1) becomes

$$g=e^{-\beta\phi+N}, \tag{2.4}$$

and when we set Z equal to -1, Eq. (2.1) becomes

$$g=e^{-\beta\phi}(1+N). \tag{2.5}$$

Equations (2.4) and (2.5) in conjunction with (2.2) give the CHNC[4–7] and PY[2,17,18] equations, respectively. Writing the equations in this form shows that equating Z to any values between 0 and -1 would have as much validity as the PY and CHNC equations. At low temperatures for LJ-type potentials, Z equated to zero gives better distribution functions.[1,18] In fact a comparison of the computed g's from the PY and CHNC integral equations with the Monte Carlo computations of Wood, Parker, and Jacobson[19] at 126°C for argon suggests that a value of Z slightly greater than zero might give even a better computed g than the CHNC approximation. This is so because the CHNC g is bracketed by the PY g and the Monte Carlo g.[1] This will also be seen from our comparisons of the computed g's with the experimental g's at low temperatures for krypton and will be discussed in the next section. A similar comparison of the computed g's by Broyles

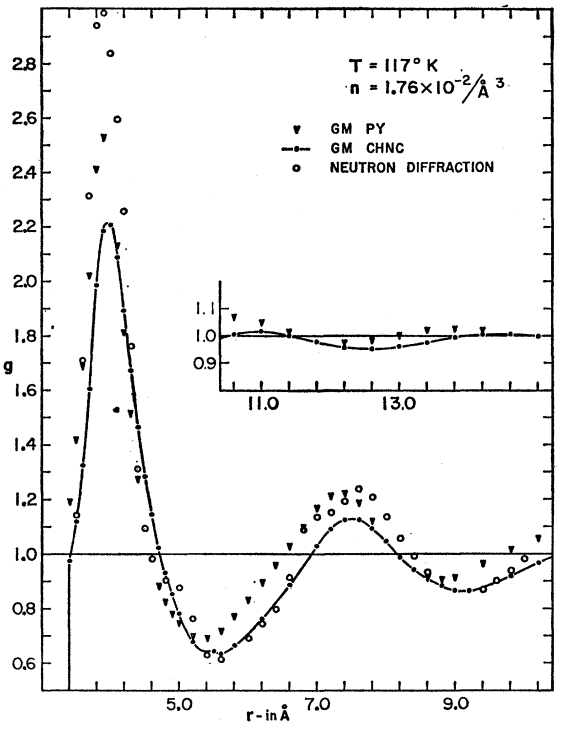

FIG. 1. The computed g's with the GM potential and the CHNC and PY equations at 117°K. The neutron diffraction points are due to Clayton and Heaton.

et al.[20] with the Monte Carlo g's of Wood and Parker[21] for densities of argon ($na^3=1$, where n is the density of particles and a is the value of r where the potential crosses the zero axis) 2.53×10^{-2} atoms/Å^3 or less show that an approximation in which the value of Z is somewhat greater than -1 will give better g's. The value -0.7292, which is the ratio of the contribution due to two-field-point elementary diagrams to that due to the two-field-point composite diagram for hard spheres,[22] would give a better approximation for hard spheres as well as for LJ-type potential at high temperatures. This is so because this value of Z considerably improves the value of the fourth virial coefficients (for hard spheres) computed from the pressure equation, and also gives better values for the fifth and sixth virial coefficients than are given by the approximation[22] $Z=-1$. The improvement shown by the approximation $Z=-0.7292$ in the values of the fourth, fifth, and sixth virial coefficients means that this approximation will take care of the elementary diagrams at least up to four field points more accurately than the PY approximation. Nothing can be said about the five-or-more-field-point elementary diagrams, as the seventh and higher

[15] See Ref. 4, Eqs. (11a) and (29).
[16] See Ref. 4 or 1 for definitions.
[17] G. Stell, Physica **29**, 517 (1963).
[18] L. Verlet and D. Levesque, Physica **28**, 1124 (1962).
[19] W. W. Wood, F. R. Parker, and J. D. Jacobson, Nuovo Cimento Suppl. **9**, 133 (1958).
[20] A. A. Broyles, S. U. Chung, and H. L. Sahlin, J. Chem. Phys. **37**, 2462 (1962); A. A. Broyles, *ibid.* **35**, 493 (1961).
[21] W. W. Wood and F. R. Parker, J. Chem. Phys. **27**, 720 (1957).
[22] P. Hutchinson and G. S. Rushbrooke, Physica **29**, 675 (1963). G. S. Rushbrooke and P. Hutchinson, *ibid.* **27**, 647 (1961). For the sixth coefficient see G. S. Rushbrooke, J. Chem. Phys. **38**, 1262 (1963).

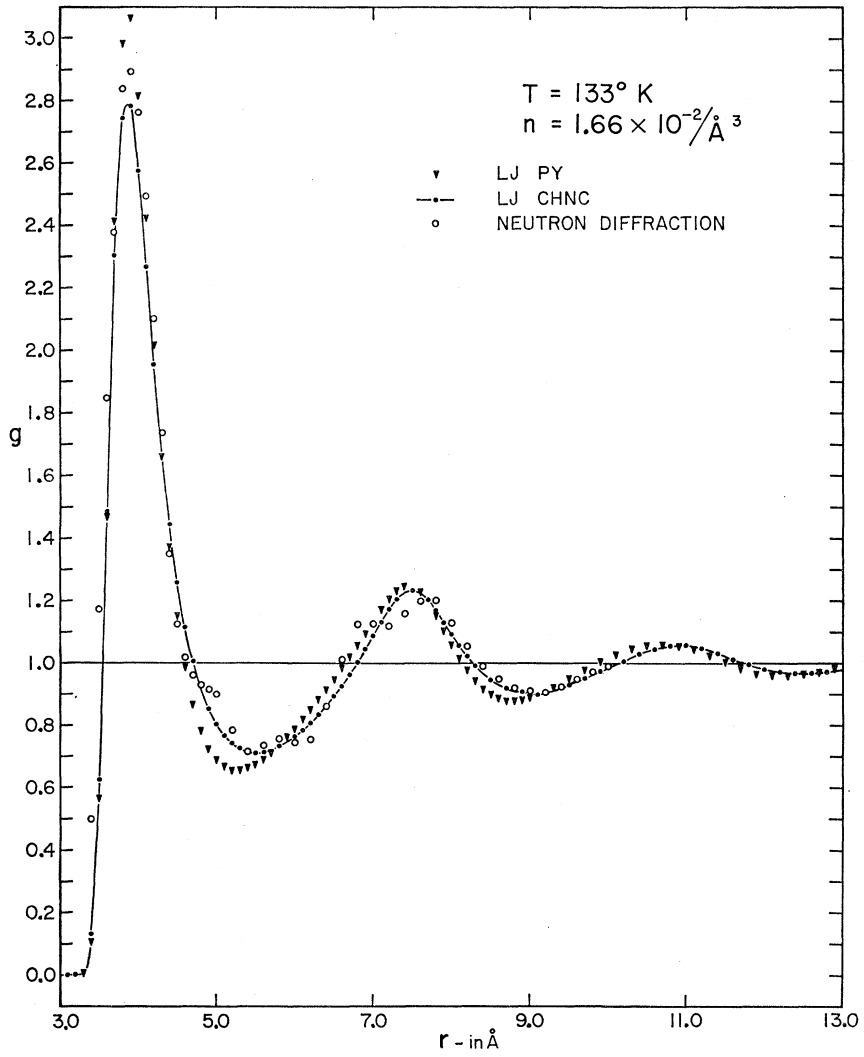

FIG. 2. The computed g's with the LJ potential and the CHNC and PY equations at 133°K. The neutron diffraction points are due to Clayton and Heaton.

virial coefficients are not known. A study of the highest density ($na^3=10/9$, or 2.82×10^{-2} atoms of argon/Å^3) distribution function computed by Broyles *et al.*[20] shows that a value of Z greater than -1 will give poorer agreement with the Monte Carlo curve[21] than $Z=-1$. Since the PY curve is bracketed everywhere by the Monte Carlo and the CHNC curve, it follows that a value of Z less than -1 will probably give a better g for this case. However, there is no simple criterion to determine the approximate value of Z except comparison of the computed results with some known distribution function. A value estimated from such a comparison will give a better approximation over a certain range of temperature and density only.

III. THE COMPUTED DISTRIBUTION FUNCTIONS

A. Computed g's and Their Comparison with the Experimental g's

Radial distribution functions of liquid krypton have been computed in the convolution-hypernetted-chain (CHNC) and Percus-Yevick (PY) approximations ($Z=0$ and $Z=-1$, respectively). The method of computation is described in Refs. 20 and 23. Since the integral equations are solved by a process of iteration, some sort of measure is required in order to estimate the convergence of the solution obtained. For this purpose the root-mean-square value of the change in the estimate of H is defined by the relation,[23]

$$\text{rms}=\left[\frac{1}{M}\sum_{j=0}^{M}\{H_{\text{in}}(j\Delta)-H_{\text{out}}(j\Delta)\}^2\right]^{1/2}, \quad (3.1)$$

where Δ is the interval of numerical integration. The g is related to H for the PY equation by[20]

$$g_{\text{PY}}=(1+H_{\text{PY}}r^{-1})\exp(-\phi/kT), \quad (3.2)$$

and for the CHNC equation by[20]

$$g_{\text{CHNC}}=\exp(H_{\text{CHNC}}r^{-1})\exp(-\phi/kT). \quad (3.3)$$

[23] A. A. Kahn, Ph.D. thesis, 1963 (unpublished).

The subscripts "in" and "out" on H correspond to the trial H and the H which is obtained from this trial H, respectively.

The computations have been done near the critical temperature ($T_c=209.4°K$) and below the critical temperature. All the densities are higher than the critical density ($n_c=6.53\times10^{-3}$ atoms/Å^3). Two different interaction potentials, (i) the Lennard-Jones 6-12 potential with constants due to Beattie, Barriault, and Brierley[11] and (ii) the Guggenheim-McGlashan potential (see Appendix) have been used. The computed g's are plotted in Figs. 1–8.

From the g's we have computed the quantity $i(s)$ which is equal to $[I(s)/I_0]-1$, where $I(s)$ is the total intensity of scattering (number of counts/min) at the angle 2θ from the direct beam, and I_0 is the constant intensity of scattering at large angles. The variable s is given by the relation

$$s=4\pi k=4\pi[(\sin\theta)/\lambda]=k'/4\pi, \tag{3.4}$$

where θ is half the angle of scattering and λ is the wavelength of the neutrons.[24] The intensity function $i(s)$ is related to $g(r)$ by the equation[25]

$$si(s)=4\pi n\int_0^\infty r[g(r)-1]\sin srdr, \tag{3.5}$$

where n is the macroscopic density of particles. The computed i's are plotted against k in Figs. 9–17.

The quantities E'/nkT, P/nkT, and $nkTK$, where E' is the internal potential energy, P is the pressure, and K is the isothermal compressibility, have also been computed from the g's. The quantities[26,27] E', P, and K are given by the equation

$$E'/nkT=(2\pi n/kT)\int_0^\infty \phi gr^2dr, \tag{3.6}$$

$$P/nkT=1-(2\pi n/3kT)\int_0^\infty \phi' gr^3dr, \tag{3.7}$$

and

$$nkTK=1-4\pi n\int_0^\infty (1-g)r^2dr, \tag{3.8}$$

respectively. For the case of the GM potential, Eq. (3.7) is replaced by the equation[23]

$$P/nkT=1-(2\pi n/3kT)\int_0^\infty \phi' gr^3dr+(2\pi/3)d^3g(d^+), \tag{3.9}$$

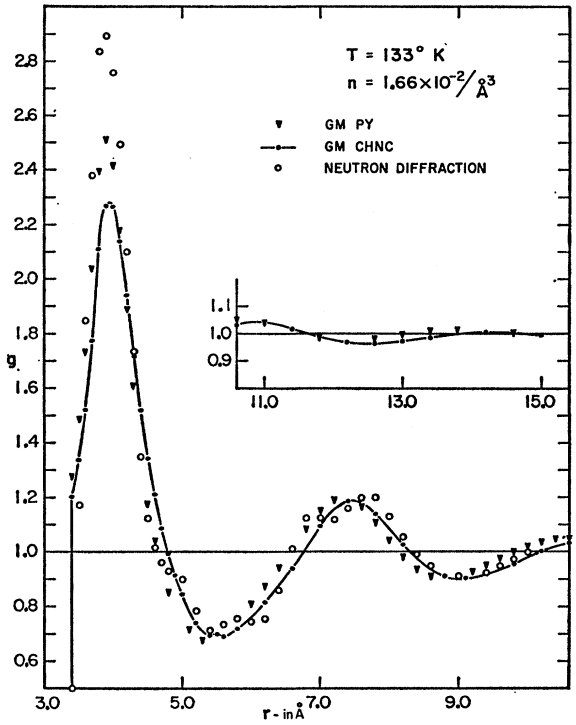

FIG. 3. The computed g's with the GM potential and the CHNC and PY equations at 133°K. The neutron diffraction points are due to Clayton and Heaton.

where $g(d^+)$ is the value of the distribution function on the right side of the vertical barrier of the GM potential. In the above equations, N is the total number of particles in the system, n is the number of particles per unit volume, and ϕ is the interatomic potential. Table I contains the computed energies, pressures, and compressibilities. The range of integrations (R) for solving the equations and the rms values are also given in the table. The computed thermodynamic quantities, particularly the pressure and the compressibility, are so sensitive to small changes in the g and also the range of g (especially the compressibility) that the computed values in many cases can be considered good only for comparative study.

For the purpose of comparison, the g's computed from the two integral equations and the experimental g's determined from the neutron diffraction experiments by Clayton and Heaton have been plotted on the same figures. In plotting the curves, care has been taken to show distinctly the two computed values and the expeirmental value of g at a given value of r (r is in angstroms). This was necessary in view of the rapid rise and fall of the g's, particularly at the first peak. The g's computed from the two different interaction potentials are plotted on separate graphs. Figure 18 shows the two potentials compared to each other. We have not

[24] Wavelength of the neutrons used by Clayton and Heaton was 1.05 Å.
[25] N. S. Gingrich, Rev. Mod. Phys. **15**, 90 (1943).
[26] R. L. Hill, *Statistical Mechanics* (McGraw-Hill Book Company, Inc., New York, 1956).
[27] L. D. Landau and E. M. Lifshitz, *Statistical Physics* (Addison-Wesley Publishing Company, Inc., Reading, Massachusetts, 1958).

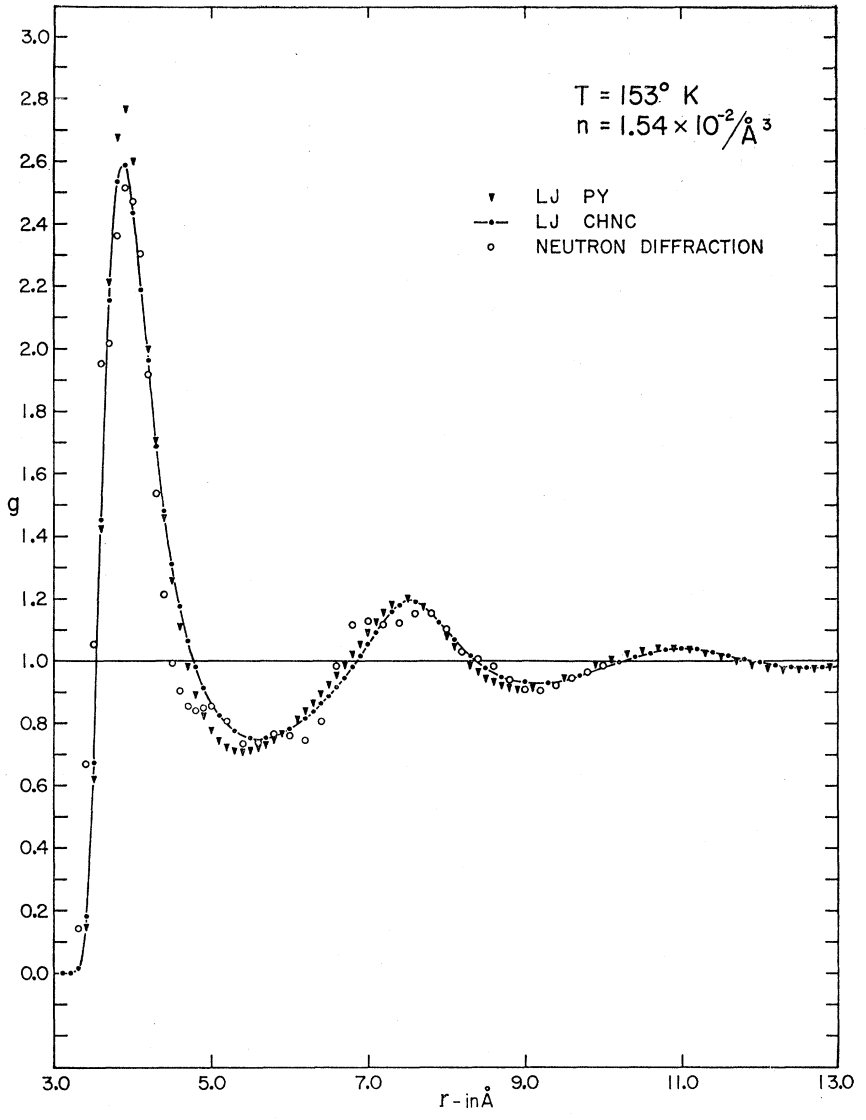

FIG. 4. The computed g's with the LJ potential and the CHNC and PY equations at 153°K. The neutron diffraction points are due to Clayton and Heaton.

been able to get the CHNC case-I-type[1,28] solutions with GM potential in the case of $T=153$°K and $T=133$°K. The solutions obtained at 117°K with the GM potential and with the PY and CHNC equations are poorly converged. Since the GM potential has a vertical barrier at 3.4 Å, the value of g is zero for values of $r<3.4$ Å. The value on the right side of the barrier is denoted in the tables by $g(d^+)$. The height of the first peak for the GM potential is lower than that for the LJ potential in all the cases.[29] (We did not get g's with the GM potentials at 210°K.) The first peak occurs at 3.9 Å for both the potentials (we are not considering the GM and CHNC, case-II solutions) except for the cases of $T=210$°K, LJ potential and the PY equation and also for $T=183$°K and $T=117$°K with the GM potential and CHNC equation. In these cases, the peak is at 4 Å. In Table I are given the positions and the heights of the first and second maxima and minima.

A comparison of the g's computed with the GM potential using either of the integral equations with the experimental g shows that the agreement is not good at the first peak for the cases of $T=117$°K, $T=133$°K, and $T=153$°K. The computed first peaks are too low. In the 117°K case, the agreement between the GM-

[28] It has been found that the CHNC equation gives two different kinds of distribution functions as solutions. One of them approaches the value one for large values of r from above, i.e., from values greater than one. The compressibility computed from this g is always positive. We consider this kind of g the valid solution and designate it as case-I g. The other g approaches the value one for large values of r from below, i.e., from values less than one. This g gives negative compressibility. We consider this kind of g the invalid solution and designate it as case-II g. See Sec. III B and Ref. 1 for further information on case-I and case-II g's.

[29] See Ref. 1.

TABLE I. Range, rms, energies, pressures, compressibilities, positions and heights of first and second maxima and minima in $g(r)$ and $g(d^+)$. T is the temperature in degrees Kelvin, n is the number of particles per cubic angstrom, Pt=potential, Eq.=equation, r_1 is the position of the first maximum in g, r_2 is the position of the first minimum in g, r_3 is the position of the second maximum in g, r_4 is the position of the second minimum in g, $g(d^+)$ is the value of g on the right side of the barrier of the GM potential.

T	$n\times10^2$	Pt	Eq.	R(Å)	rms	$\frac{E'}{nkT}$	$\frac{P}{nkT}$	$nkTK$	r_1	$g(r_1)$	r_2	$g(r_2)$	r_3	$g(r_3)$	r_4	$g(r_4)$	$g(d^+)$
210	0.75	LJ	PY	20	5.7×10^{-4}	−2.119	0.24	6.00	4.0	2.1868	6.0	0.9614	7.8	1.1247	9.9	1.0327	
		Neutron diffraction experiment							4.1	2.62	6.1	0.64	8.0	1.11			
183	1.30	LJ	PY	30	4.0×10^{-3}	−3.931	0.41	0.80	3.9	2.396	5.6	0.789	7.6	1.136	9.2	0.953	
		LJ	CHNC	30	1.7×10^{-3}	−3.926	0.35	1.54	3.9	2.308	5.8	0.816	7.6	1.130	9.4	0.963	
		GM	PY	30	3.8×10^{-4}	−3.230	1.40	2.03	3.9	2.1412	5.6	0.7753	7.5	1.1311	9.1	0.9571	1.1879
		GM	CHNC	30	2.5×10^{-4}	−3.297	1.29	7.98	4.0	2.1193	5.6	0.7957	7.6	1.1527	9.3	0.9701	1.2313
		Neutron diffraction experiment							4.0	2.22	6.3	0.77	7.6	2.00			
	1.32	LJ	PY	30	1.4×10^{-3}	−3.988	0.41	0.78	3.9	2.396	5.6	0.788	7.6	1.137	9.2	0.952	
		LJ	CHNC	30	1.5×10^{-3}	−3.977	0.42	1.28	3.9	2.318	5.8	0.812	7.6	1.132	9.4	0.961	
153	1.54	LJ	PY	30	2.7×10^{-4}	−5.620	0.80	0.35	3.9	2.7685	5.4	0.7103	7.5	1.2006	8.9	0.9130	
		LJ	CHNC	30	3.6×10^{-3}	−5.583	0.73	0.58	3.9	2.589	5.6	0.751	7.5	1.190	9.1	0.931	
		GM	PY	20	4.0×10^{-3}	−4.519	2.03	0.54	3.9	2.342	5.4	0.710	7.4	1.170	8.9	0.925	1.260
		GM	CHNC II	30	2.4×10^{-2}	−4.587	1.25	−6.94	4.0	2.18	5.4	0.75	7.5	1.16	9.2	0.93	1.17
		Neutron diffraction experiment							3.9	2.51	5.4	0.74	7.7	1.16	9.1	0.90	
133	1.66	LJ	PY	30	1.2×10^{-3}	−7.022	1.19	0.23	3.9	3.065	5.3	0.659	7.4	1.245	8.8	0.881	
		LJ	CHNC	30	7.0×10^{-3}	−6.979	0.91	0.41	3.9	2.787	5.5	0.713	7.5	1.235	9.0	0.908	
		GM	PY	30	6.0×10^{-3}	−5.583	2.57	0.63	3.9	2.511	5.3	0.678	7.3	1.198	8.8	0.905	1.276
		GM	CHNC II	30	1.9×10^{-2}	−5.661	1.51	−8.30	3.9	2.27	5.6	0.69	7.5	1.19	9.1	0.91	1.20
		Neutron diffraction experiment							3.9	2.89	5.4	0.72	7.7	1.21	9.2	0.91	
117	1.76	LJ	PY	30	7.9×10^{-3}	−8.153	1.52	0.17	3.9	3.330	5.1	0.617	7.4	1.283	8.7	0.853	
		LJ	CHNC	30	8.2×10^{-3}	−8.460	0.73	0.23	3.9	2.985	5.4	0.677	7.5	1.279	8.9	0.884	
		GM	PY	30	1.2×10^{-1}	−6.585	2.56	6.56	3.9	2.5	5.5	0.7	7.3	1.2	8.8	0.9	1.2
		GM	CHNC	30	1.3×10^{-2}	−6.493	0.94	12.44	4.0	2.21	5.6	0.63	7.5	1.13	9.1	0.87	0.98
		Neutron diffraction experiment							3.9	3.00	5.6	0.61	7.7	1.24	9.2	0.86	

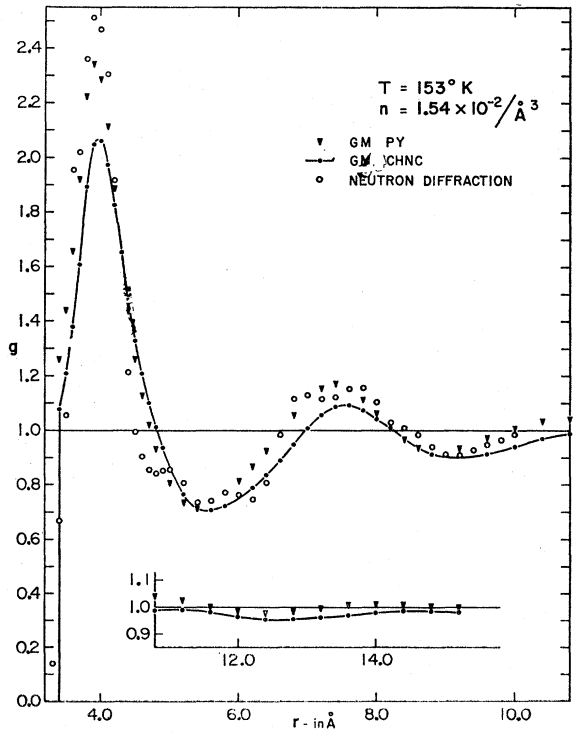

FIG. 5. The computed g's with the GM potential and the CHNC and PY equations at 153°K. The neutron diffractions points are due to Clayton and Heaton.

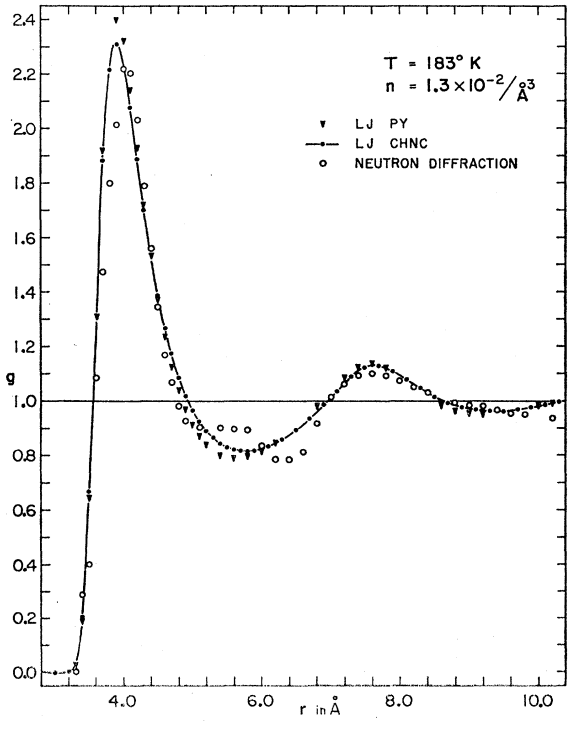

FIG. 6. The computed g's with the LJ potential and the CHNC and PY equations at $T=183$°K. The neutron diffraction points are due to Clayton and Heaton.

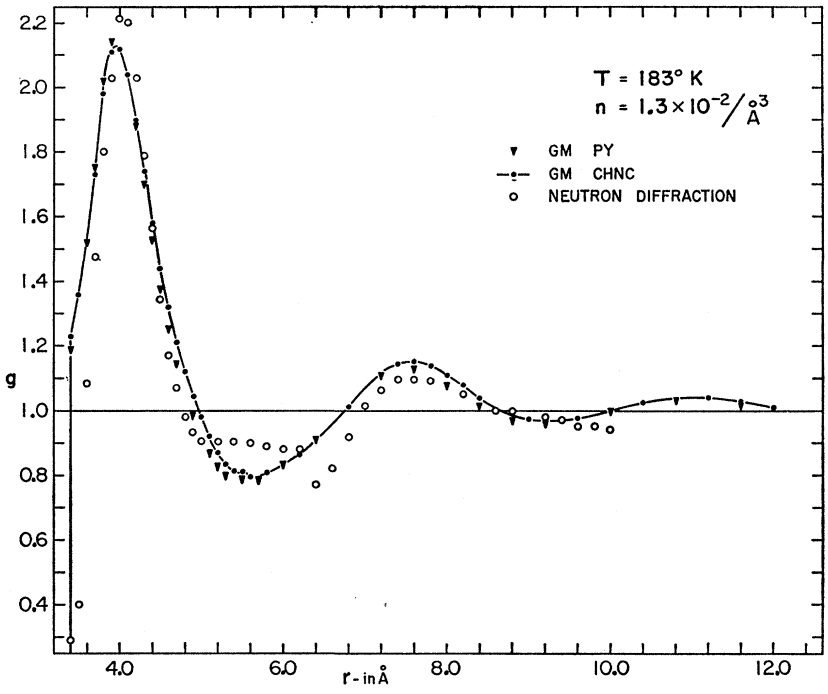

FIG. 7. The computed g's with the GM potential and the CHNC and PY equations at $T=183°K$. The neutron diffraction points are due to Clayton and Heaton.

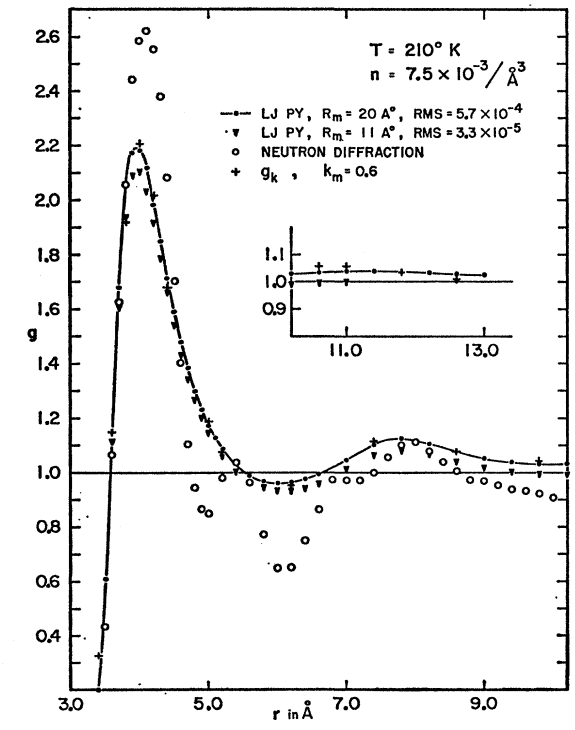

FIG. 8. The computed g's with the LJ potential and the PY equation for the ranges of integration of 20 and 11 Å. Root-mean-square (rms) value is a measure of convergence of the solutions (see text). The g_k points have been obtained by converting the LJ-PY (range 20 Å) curve first into an intensity $i(k)$ versus $k[k=(\sin\theta)/\lambda]$ curve and then reconverting the intensity curve (extending only up to $k=0.6$ Å^{-1}) into a distribution curve. The neutron diffraction points are due to Clayton and Heaton.

CHNC curve and the experimental points is better near the first and second minima than elsewhere, while the GM-PY curve is close to the experimental points at the second maxima (see Fig. 1). In the 133°K case, both the computed curves with the GM potential show fairly good agreement with the experimental curve near and beyond the first minima. In this region the GM-CHNC curve is bracketed by the experimental points and the GM-PY curve (see Fig. 3). For the case of 153°K computed g's, the situation resembles that of the 117°K case (see Fig. 5). In the case of 183°K, the PY and CHNC equations with the GM potential give g's which are very close to each other, and they are also in good agreement with the experimental points at the first peak. The location of the first peak for the GM-CHNC case is at 4 Å (while in other cases it is at 3.9 Å), which is in agreement with the location of the experimental peak (see Fig. 7). It may be noticed that there are irregularities in the experimental curve near the first minimum and the second maximum which make the comparisons with the computed curve difficult. We shall discuss these irregularities of the experimental curves in Sec. IV.

The distribution functions computed using the LJ potential are in better accord with the experimental curves in all the cases than those computed with the GM potential. For the 117°K case, the LJ-CHNC curve agrees better at the first peak with the experimental curve than in any other case. The agreement near and beyond the first minimum is fairly good. In this region the LJ-CHNC curve lies between the experimental points and the LJ-PY points (see Fig. 19). For 133°K

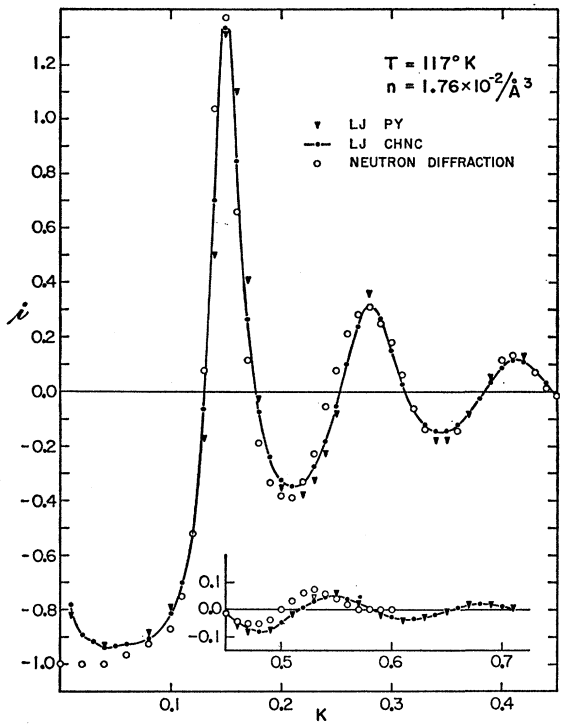

FIG. 9. The computed i's with the LJ potential and the CHNC and PY equations at 117°K. The neutron diffraction points are due to Clayton and Heaton.

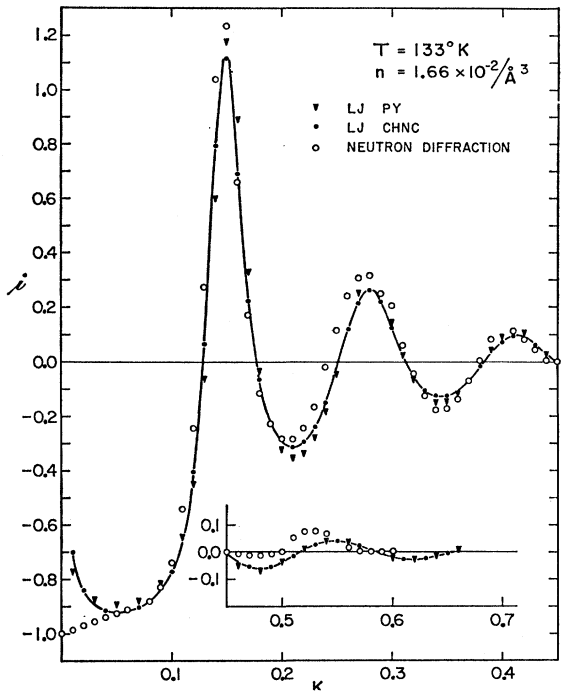

FIG. 11. The computed i's with the LJ potential and the CHNC and PY equations at 133°K. The neutron diffraction points are due to Clayton and Heaton.

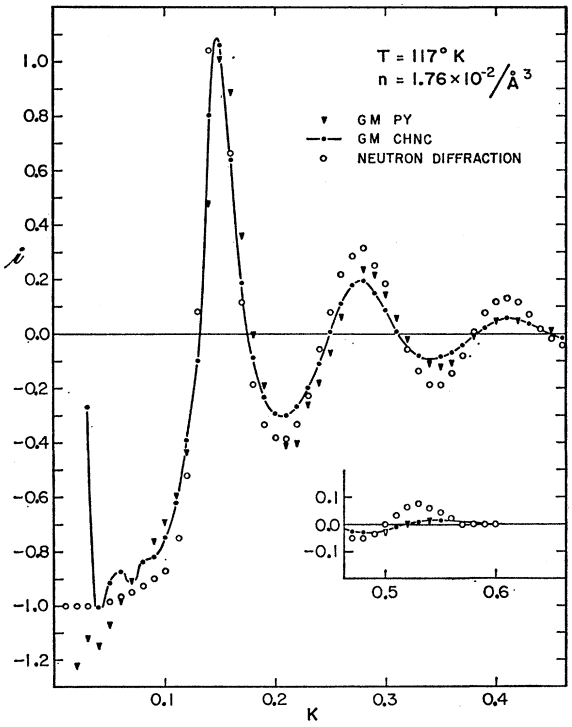

FIG. 10. The computed i's with the GM potential and the CHNC and PY equation at 117°K. The neutron diffraction points are due to Clayton and Heaton.

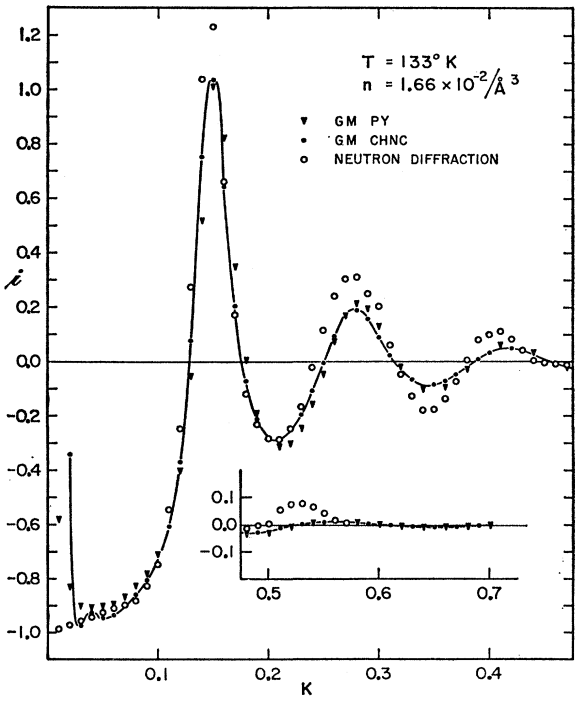

FIG. 12. The computed i's with the GM potential and the CHNC and PY equations at 133°K. The neutron diffraction points are due to Clayton and Heaton.

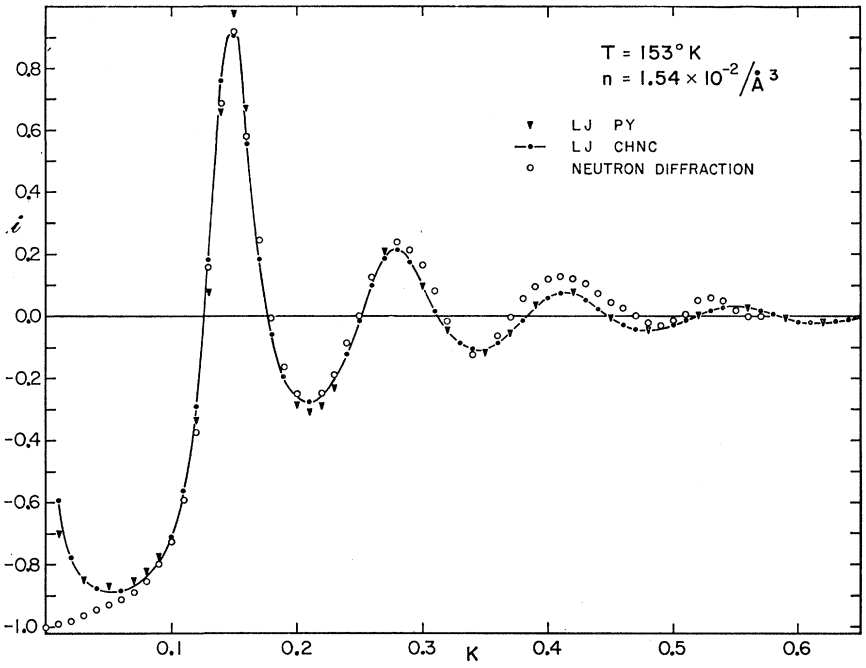

FIG. 13. The computed i's with the LJ potential and the CHNC and the PY equation at 153°K. The neutron diffraction points are due to Clayton and Heaton.

the agreement between the experimental points and the LJ-CHNC curve near and beyond the first minimum is even better than in the case of 117°K. In this region the LJ-CHNC curve lies between the LJ-PY curve and the experimental points except beyond 9 Å. There the experimental points are almost on the LJ-CHNC curve. The experimental points in this case are higher than the LJ-CHNC curve and lower than the LJ-PY curve at the first peak (see Fig. 2). At the 153°K case the agreement between the LJ-CHNC curve and the experimental points is very good. The LJ-PY curve is very close to the LJ-CHNC curve in this region. The experimental first peak is a little lower than the LJ-CHNC peak. It is also a little shifted to the right of the LJ-CHNC and the LJ-PY peaks. The LJ-PY peak is much higher than the experimental peak (see Fig. 4). At 183°K, the experimental peak is close to 4 Å, while both the LJ-PY and LJ-CHNC peaks are near 3.9 Å.

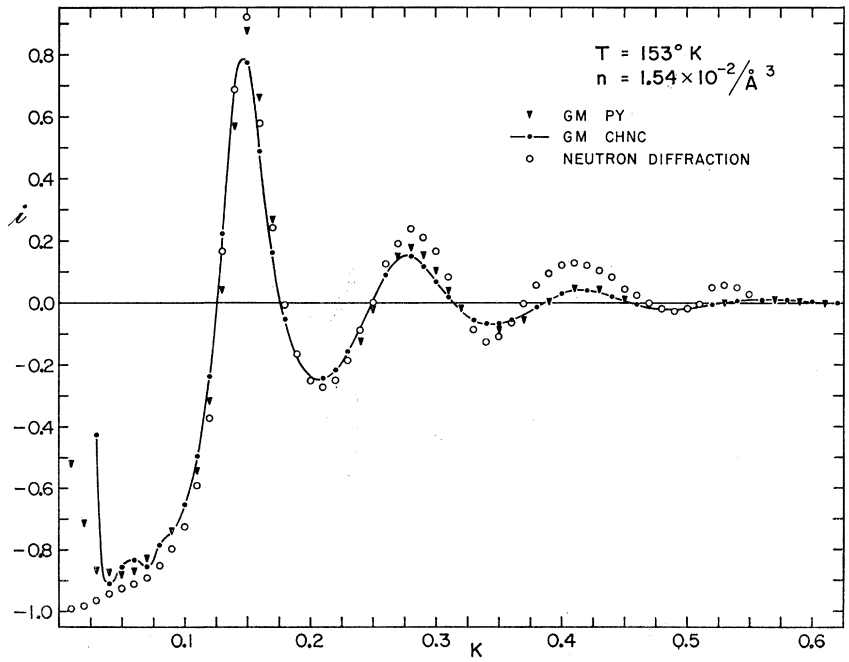

FIG. 14. The computed i's with the GM potential and the CHNC and PY equations at 153°K. The neutron diffraction points are due to Clayton and Heaton.

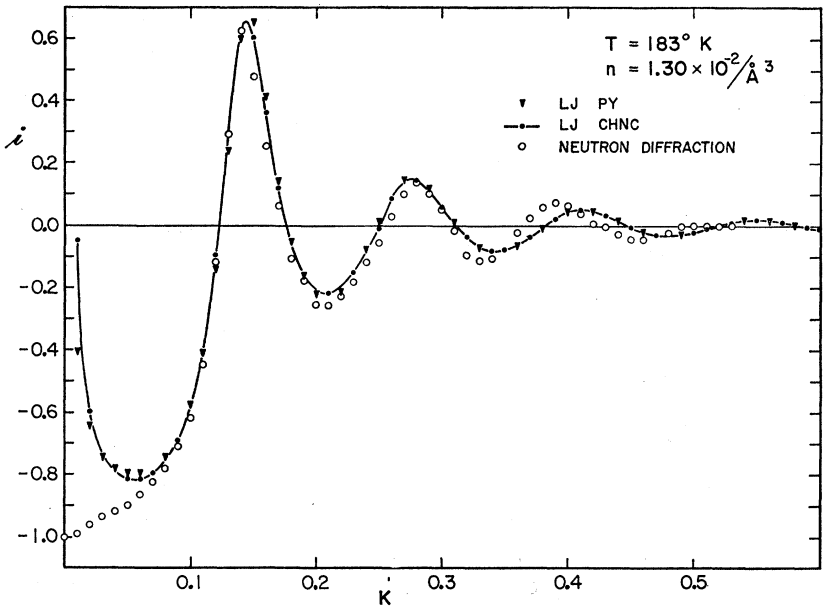

FIG. 15. The computed i's with the LJ potential and the CHNC and PY equations at 183°K. The neutron diffraction points are due to Clayton and Heaton.

Also, the experimental peak is lower than the LJ-CHNC peak, which in turn is lower than the LJ-PY peak. The LJ-PY and LJ-CHNC curves are very close in this case and in good agreement with the experimental points (see Fig. 6).

From the study of computed g's discussed above, it is clear that the LJ-CHNC curves are in better agreement with the experimental points than any other curves. Since the CHNC and PY approximations correspond to $Z=0$ and $Z=-1$, respectively (see Sec. II), it appears, from our comparisons of the LJ-CHNC and LJ-PY curves with the experimental curves in the cases of 117 and 133°K, that if we solve for g in an approximation in which Z is slightly greater than zero, then we may get even better agreement with the experimental points than the CHNC approximation for regions beyond 4.6 Å. But such an approximation may make the agreement at the first peak poorer than we get from the $Z=0$ approximation. From this it follows that no further improvement in the computed g's can be expected just by approximating Z to a constant slightly greater than zero. However, an improvement can be obtained if we obtain approximate values of Z as a function of the distance.[30]

At 210°K, we obtained solutions with the LJ potential and the CHNC and the PY equations for a range of integration of 11 Å. The PY and the CHNC solutions are very close to each other. The LJ-PY curve for $R=11$ Å has been plotted in Fig. 8. We could not get solutions with the CHNC equation for larger ranges. With the PY equation we got a solution for a range of 20 Å also, but when we tried to extend the range to 30 Å we did not get a well converged solution. The increase in range in this case increases the g almost

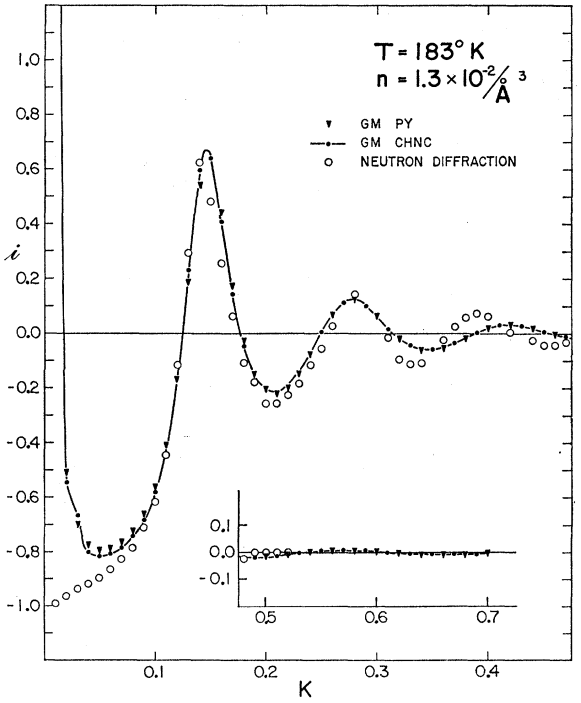

FIG. 16. The computed i's from the GM potential and the CHNC and PY equations at 183°K. The neutron diffraction points are due to Clayton and Heaton.

[30] Verlet and Levesque (Ref. 18) have computed the ratio of the contribution of the two-field-point elementary diagrams to the two-field-point composite diagram for various separations of the reference points for hard spheres. This ratio may serve as a good value of z as a function of r for cases close to hard spheres. Such ratios can be determined for the LJ or the GM-type pair potentials using Monte Carlo methods. However, this is expected to give good results as long as the contribution due to more-than-two-field-point elementary diagrams is negligible. The extension of such calculations to diagrams with a large number of field points would be very cumbersome.

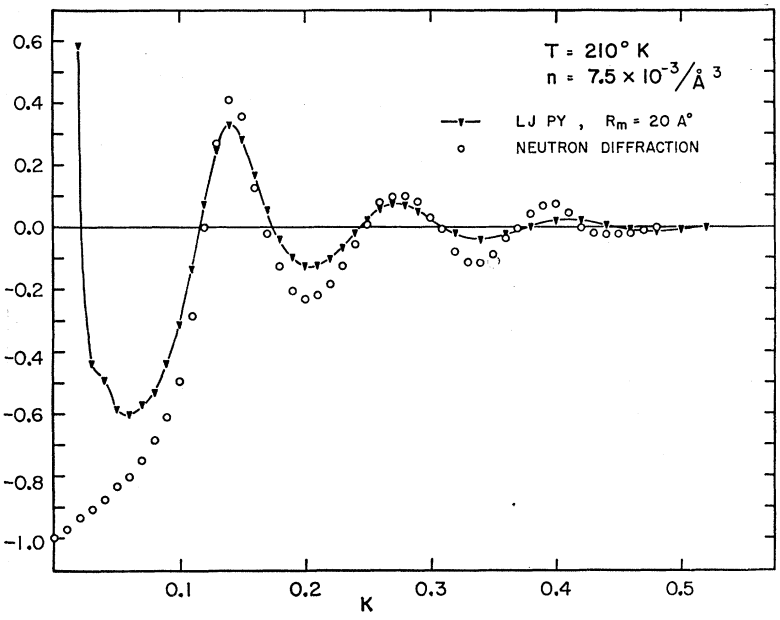

FIG. 17. The computed $i(s)$ with the LJ potential and the PY equation at 210°K. This intensity curve is computed from the g which extends up to 20 Å. The neutron diffraction points are due to Clayton and Heaton.

everywhere (see Fig. 8). It appears that a well-converged solution for a longer range will result in a g with a little higher value than the g obtained for the range of 20 Å. Although we could not get the solutions for the CHNC equation for longer ranges than 11 Å, we expect the CHNC solutions for longer ranges to be close to the PY solutions, as in the case of 11 Å. A comparison of the computed curves with the experimental points shows that there is some agreement so far as the location of the first and second maxima is concerned. There also may be agreement in the location of the first minimum if the experimental curve is smoothed out in that region. Otherwise the agreement is very poor. At this temperature, minor changes in the potential function cannot cause much difference in the computed curves. Computed g's for argon[1] near the critical temperature (at densities lower and higher than the critical density) are also not in agreement with the x-ray diffraction curves.[9] A comparison of the neutron diffraction curve for krypton and the x-ray diffraction curve for argon in the neighborhood of the first peak shows that while the neutron diffraction shows a sharper and much higher peak than the computed peaks, the x-ray diffraction shows a smeared-out and much lower peak than the computed peaks.[1] The computed curves for krypton and the argon are similar to each other. From this it appears that both the neutron diffraction and the x-ray diffraction experimental g's for krypton and argon, respectively, near the critical temperature are not as reliable as the computed g's from the integral equations.

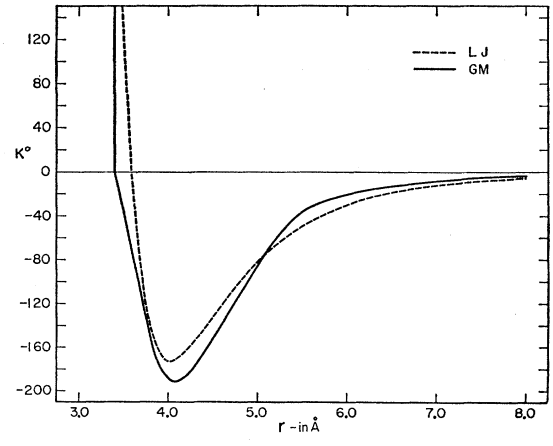

FIG. 18. The Lennard-Jones (with constants due to Beattie *et al.*) 6-12 and the Guggenheim-McGlashan potential for krypton. The distance is in angstroms and the energy in degrees Kelvin.

Figures 9 and 11 show the computed intensity (i) curves with the LJ potential, the experimental i's for the cases of 117 and 133°K, respectively. The computed curves are in good agreement with the experimental points. In the region lying between the first minimum and the second maximum the experimental curves are markedly shifted towards the left relative to the computed curves. Also, the agreement between the computed and experimental curves is poor in the neighborhood of $k=0.5$ Å^{-1}. The fourth experimental peak is very much shifted towards the left. At 153°K, the experimental points are too high near the third maximum, and the fourth maximum is shifted towards the left of the fourth maximum of the computed curves (see Fig. 15). For these three cases, the computed curves obtained from the CHNC equation show an over-all better agreement with the experimental curves than the curves computed from the PY equation. The experimental curves become out of phase with the computed curves near the third maximum in the cases

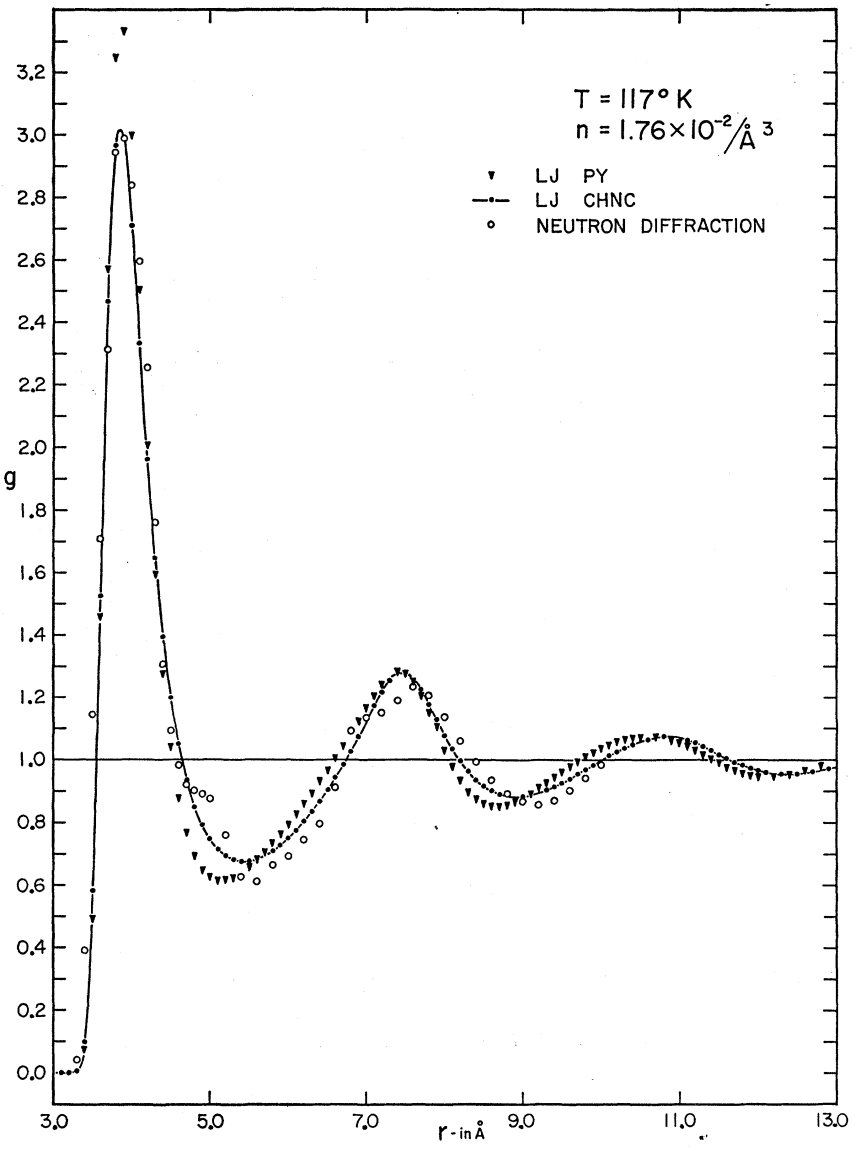

FIG. 19. The computed g's with the LJ potential and the CHNC and PY equations at 117°K. The neutron diffraction points are due to Clayton and Heaton.

of 183 and 210°K. The agreement between the experimental curve and the computed curves is fairly good up to $k=0.31$ Å^{-1} for 183°K case, but for the 210°K case the agreement is only qualitative (see Figs. 15 and 17).

In all the cases discussed above the computed i curves for small values of k pass through a minimum and again start rising. As the temperature increases the value of i for very small values of k becomes quite high and, at the critical temperature, this small-angle scattering is much larger than that at the first maximum. The experimental measurements were not made at very small angles, and the values of i for small k were obtained by extrapolation.[8] Since the zero-angle scattering intensity $i(0)$ is related to the compressibility K by the equation,

$$1+i(0)=nkTK, \tag{3.10}$$

it might be thought that an experimental estimate of the isothermal compressibility K may be of help in the determination of the scattering intensity in the neighborhood of $k=0$. However, it turns out to be of not much use. In Sec. IV we have described the effect of the values of i for small values of k on the g's.

The agreement between the experimental i curves and the curves computed with the GM potential is not as good as it is for the curves computed with the LJ potential (see Figs. 10, 12, 14, and 16).

A comparison[1] of the pressures and compressibilities computed from the PY and CHNC equations shows that the PY equation gives higher pressures and lower compressibilities than the CHNC equation. The energies computed from the PY equation with the LJ potential are lower than those computed from the CHNC equation with the LJ potential. A similar com-

TABLE II. Range, rms, energies, pressures, compressibilities, positions and heights of first and second maxima and minima in $g(r)$ and $g(d^+)$. T is the temperature in degrees Kelvin, n is the number of particles per cubic angstrom, Pt=potential, Eq.=equation, r_1 is the position of the first maximum in g, r_2 is the position of the first minimum in g, r_3 is the position of the second maximum in g, r_4 is the position of the second minimum in g, $g(d^+)$ is the value of g on the right side of the barrier of the GM potential.

T	$n\times10^2$	Pt	Eq.	R(Å)	rms	$\frac{E'}{nkT}$	$\frac{P}{nkT}$	$nkTK$	r_1	$g(r_1)$	r_2	$g(r_2)$	r_3	$g(r_3)$	r_4	$g(r_4)$	$g(d^+)$
210	0.75	LJ	PY	11	3.3×10^{-5}	1.9778	0.3817	1.58	4.0	2.1026	6.1	0.9312	7.8	1.0807	10.1	0.9922	
			CHNC	11	3.0×10^{-5}	1.9916	0.3702	1.74	4.0	2.1018	6.1	0.9405	7.8	1.0847	10.1	0.9925	
183	1.30		PY	11	3.9×10^{-4}	3.7576	0.7013	0.26	3.9	2.378	5.6	0.7981	7.6	1.1222	9.2	0.9675	
				20	8.5×10^{-5}	3.9125	0.4077	0.72	3.9	2.3855	5.6	0.7920	7.6	1.1343	9.2	0.9541	
			CHNC I	11	1.2×10^{-4}	3.7466	0.6899	0.23	3.9	2.2981	5.8	0.8177	7.6	1.1177	9.5	0.9705	
				15	3.4×10^{-5}	3.8633	0.4843	0.77	3.9	2.3084	5.8	0.8147	7.6	1.1281	9.4	0.9625	
				16	1.0×10^{-6}	3.8717	0.4683	0.91	3.9	2.3087	5.8	0.8146	7.6	1.1288	9.4	0.9619	
				20	3.5×10^{-4}	3.9050	0.3945	1.01	3.9	2.3097	5.8	0.8151	7.6	1.1294	9.4	0.9627	
			CHNC II	11	1.0×10^{-5}	3.08211	−0.4713	−5.76	4.0	1.5798	5.9	0.7429	8.1	0.9545	9.2	0.9403	
				15	4.0×10^{-4}	3.3862	−0.2681	−9.09	3.9	1.8091	5.9	0.7531	7.8	0.9648	9.4	0.9026	
				20	1.9×10^{-4}	3.5662	−0.0859	−14.34	3.9	1.9728	5.9	0.7694	7.7	1.0015	9.5	0.9035	
153	1.54	LJ	PY	20	5.1×10^{-4}	5.5912	0.8500	0.20	3.9	2.7670	5.4	0.7106	7.5	1.2005	8.9	0.9129	
			CHNC I	20	5.9×10^{-3}	5.556	0.759	0.44	3.9	2.584	5.6	0.752	7.5	1.189	9.1	0.931	
			CHNC II	20	4.9×10^{-4}	5.0666	−0.3242	−18.28	3.9	2.1625	5.7	0.7165	7.7	1.0324	9.3	0.8803	
		GM	CHNC II	20	2.5×10^{-3}	4.362	1.121	−9.91	4.0	2.062	5.4	0.715	7.5	1.094	9.2	0.899	1.076
133	1.66	LJ	PY	20	2.8×10^{-3}	6.988	1.220	−0.02	3.9	3.058	5.3	0.660	7.4	1.245	8.8	0.883	
			CHNC II	20	2.4×10^{-3}	6.368	−0.556	−19.14	3.9	2.334	5.6	0.687	7.6	1.068	9.2	0.867	
		GM	PY	20	7.3×10^{-3}	5.580	2.569	0.33	3.9	2.510	5.3	0.678	7.3	1.198	8.8	0.905	1.276
		GM	CHNC II	20	2.4×10^{-2}	5.53	1.19	−7.20	4.0	2.20	5.4	0.69	7.5	1.15	9.1	0.89	1.09

parison could not be made for the case of the GM potential, since we did not get the CHNC case-I solutions with the GM potential for the cases of 153 and 133°K, and the convergence of the solutions obtained at 117°K is not good enough for such a comparison (see Table I).

In the case of 183°K we increased the density by a small amount (from 1.30×10^{-2} to 1.32×10^{-2} atoms/Å^3); the result was an increase in the pressure and a decrease in the compressibility. However, this effect is more pronounced for the CHNC equation than the PY equation, as can be seen from the Table I.

B. Effect of the Range of Integration on the Distribution Functions in Solving the Integral Equations

Table II shows the positions and values of the first and second maxima and minima of the g's for ranges of integration (R) other than those included in Table I.

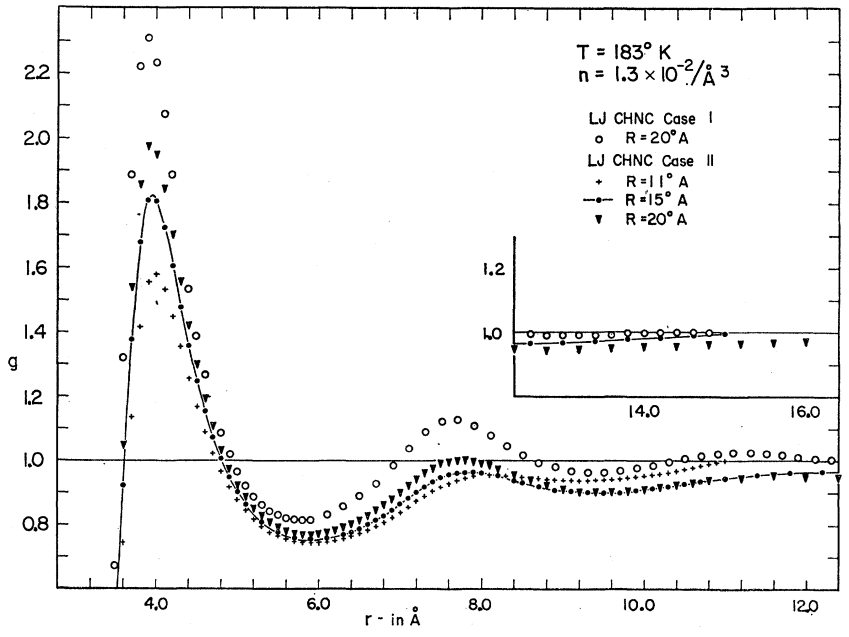

FIG. 20. The computed g's at 183°K, with the LJ potential and CHNC equation case-II type for 11-, 15-, and 20-Å ranges. The g with LJ potential and CHNC equation case I for range 20 Å is also plotted for comparison.

It also gives the values of the thermodynamic quantities computed from the g's obtained for these ranges.

There is little difference in the g's computed for 20 and 30 Å range. (See Tables I and II for the heights of the first and second maxima and minima. We are not considering the CHNC case-II solutions.) The differences in the energies and pressures are small. Their differences are mostly due to different degrees of convergence of the g's rather than the effect of range. The effect on the compressibility due to change in range from 20 to 30 Å is very large. In the case of 133°K and the LJ-PY g for range 20 Å, the compressibility is negative[31] and very small (−0.02) (see Tables I and II). The compressibilities for the range of 30 Å are much larger than those for the range of 20 Å.

At 183 and 210°K, we solved the integral equations for the range of 11 Å also. In these cases the g's have relatively lower maxima and higher minima compared to g's for the 20- to 30-Å ranges. The energies are lower, the pressures are higher, and the compressibilities are very much smaller in comparison to the 20- and 30-Å cases (see Tables I and II). For the 183°K case (LJ-CHNC, case I) we obtained solutions for the ranges of 15 and 16 Å also. It will be noticed (see Table II) that there is considerable difference in the compressibility even for a change of 1 Å in the range. From the above we conclude that the g's obtained for a range of integrations much less than 20 Å are not reliable and that the compressibilities are good only for a comparative study.

We obtained CHNC case-II-type[1,28] solution at 183°K for 11-, 15-, and 20-Å range with the LJ potential; but we did not get a solution for 30-Å range. The effect of increasing the range is to increase the distribution function almost everywhere except in the region close to the end of the range, where the shorter range g crosses the longer range g's so as to approach 1 (see Fig. 20). We obtained CHNC case-II g's in many cases Some of them are listed in Table II. Those cases which are listed in Table I have also been plotted in the distribution-function graphs. In those cases we did not get corresponding CHNC case-I-type solutions. The CHNC type-II g's give negative compressibilities and, in several cases, negative pressures also (see Tables I and II). With increase in range the compressibility increases in magnitude but continues to be negative. A comparison of the distribution functions for the different ranges corresponding to CHNC case-I and case-II solutions shows that as the range increases, the difference between case-I and case-II g's decreases in the region sufficiently far removed from the end of the range of either g.

C. Effect of Varying the Long-Range Part of the Potential Function on the Distribution Function

The form of the interaction potential at large distances for two nonpolar atoms is very well represented[32] by the London dispersion forces[10] and is proportional to r^{-6}. At low temperatures in liquids, the effect of this long-range potential may be quite important. In order to study the effects of varying the magnitude of this part of potential function, we computed the distribution functions with the GM potentials for values of $\lambda/k=0$, 100, 250, and 300°K besides the value 208.5°K. In Fig. 21 are plotted the curves computed from the PY equation with the GM potential for values of $\lambda/k=0$, 100, and 300°K. In Fig. 22 are plotted the g's computed from the CHNC equation with the GM potential for values of $\lambda/k=0$, 250, and 300°K. From these figures it can be seen that the effect of changing λ/k is rather small. The height of the first peak rises with the increase[33] in the value of λ/k. (This does not apply to the case of the g computed from CHNC equation for $\lambda/k=300$°K, because this corresponds to the CHNC case-II g.) There is irregularity in the g's near the first minimum. This irregularity is caused by the abrupt change in the potential function at 5.8 Å due to giving values to λ/k other than 208.5°K. It is interesting to note that the irregularities in the distribution curves are appearing almost exactly at the point where the deformation in the potential function takes place owing to a change in the values of λ/k. Another interesting thing is that, for values of λ/k less than 208.5°K, the value of g drops from a higher value to a lower value as it passes from 5.7 to 5.8 Å. It rises from lower values to higher values in passing from 5.7 to 5.8 Å when the value of λ/k is greater than 208.5°K. Since this fact is common to g's computed either by the PY or CHNC equations, it may be that an irregularity in the exact distribution function also shows a peculiarity in the potential function very close to that point.[34]

There is a small increase in the values of energies with the decrease in the values of λ/k. The values of the compressibilities increase considerably with the increase in the value of λ/k. See Table III.

[31] The PY g's and also the CHNC case-I type g's have never been found to give negative compressibilities. In this case it appears that the range 20 Å happens to be such that this as upper limit in the integral of Eq. (3.8) favors the values of g less than one considerably over those greater than one. This is why when the range is increased to 30 Å, the compressibility again becomes positive and relatively very large. It may be noticed that the compressibilities computed from the g's of the CHNC case-II type never become positive with a change in the range. They become more negative as the range is increased (see Table II, particularly the case of 183°K).

[32] For extremely large distances the interaction potential is actually proportional to r^{-7} because of radiation effects (finite velocity of the electromagnetic waves).

[33] This may be one factor responsible for higher first peaks for g's computed with the LJ potential, since the constant of proportionality in the r^{-6} term is greater for the LJ potential than that for the GM potential.

[34] It may be that at very high pressures in the liquid state, or at high temperatures, the irregularities of the potential function do not show up in the distribution function; or it may be weakened in prominence and displaced and spread out in position.

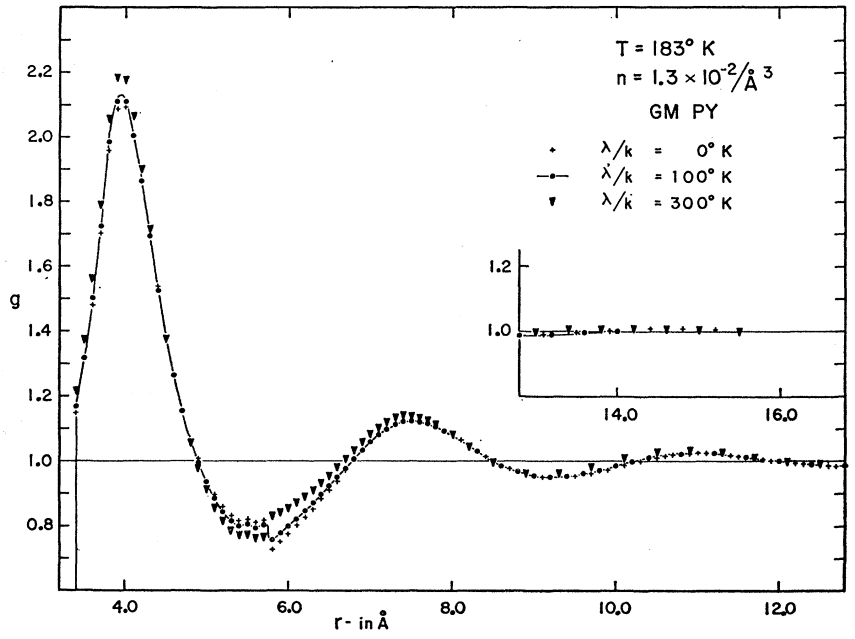

FIG. 21. The g's computed from the PY equation at 183°K with the GM potential for values of $\lambda/k=0$, 100, and 300°K. The irregularity in g's near 5.8 Å is due to the abrupt change in the potential function at 5.8 Å because of giving values to λ/k other than the 208.5°K.

IV. THE IRREGULARITIES OF THE EXPERIMENTAL g's AND THE CONCLUSIONS

A. The Irregularities in the Experimental Distribution Curves

A detailed study has been made in order to determine the causes of the irregularities in the experimental g's. In Ref. 1 we had converted the computed distribution curves first into intensity[35] J curves (J versus k curves). Then, taking these intensity curves up to those values of k ($k_{max}=0.7$) to which the experimental curves extended, we reconverted them to distribution curves and called them g_k. A comparison of the original g's with the g_k's showed that there was quite good agreement between the two cases. There was also no indication of the appearance of any wriggles or bumps in g_k. In the case of krypton, the experimental intensity curve (i versus k) extends only up to k equal to 0.6 Å^{-1} or even less.

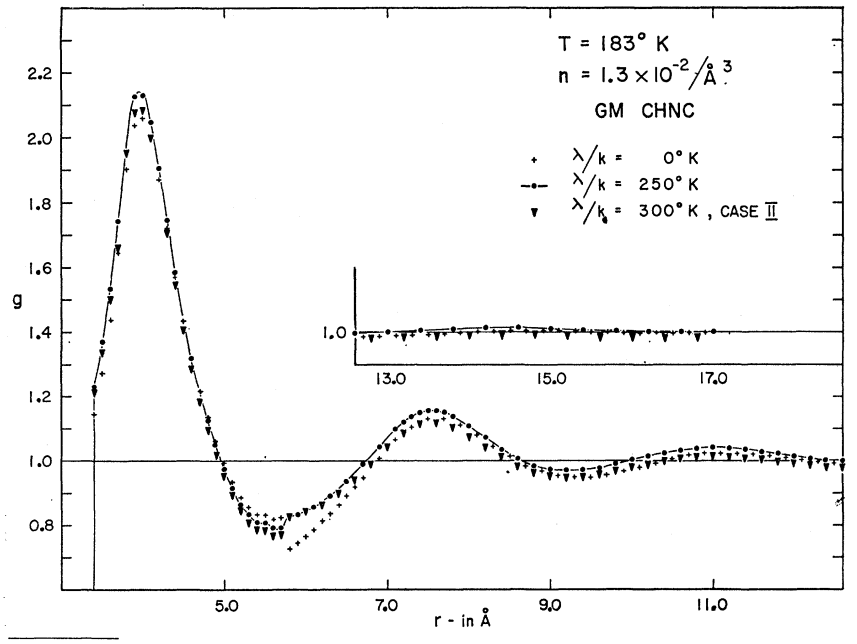

FIG. 22. The g's computed from the CHNC equation at 183°K with the GM potential for values of $\lambda/k=0$, 250, and 300°K. The g corresponding to 300°K is of case-II type. The irregularity in g's near 5.8 Å is due to abrupt change in the potential function at 5.8 Å because of giving values to λ/k other than the 208.5°K.

[35] The quantity J in Ref. 1 and $i(s)$ is related by the equation $J=[1+i(s)]f^2$, where f is the atomic structure factor.

TABLE III. Range, rms, energies, compressibilities, positions, and heights of first and second maxima and minima in $g(r)$ and $g(d^+)$ $T=183°K$, $n=1.3\times10^{-2}$ atoms/Å^3, GM potential with different values of λ/k°K. T and λ/k are in degrees Kelvin, Eq.=equation, r_1 is the position of the first maximum in g, r_2 is the position of the first minimum in g, r_3 is the position of the second maximum in g, r_4 is the position of the second minimum in g, $g(d^+)$ is the value of g on the right side of the barrier of the GM potential. The long-range part of the potential is given by $-\lambda(4.077/r)^6$. It starts being effective at $r=5.8$ Å.

Eq.	λ/k	R(Å)	rms	$\frac{E'}{nkT}$	$nkTK$	r_1	$g(r_1)$	r_2	$g(r_2)$	r_3	$g(r_3)$	r_4	$g(r_4)$	$g(d^+)$
PY	300	20	4.7×10^{-3}	3.289	2.74	3.9	2.181	5.6	0.763	7.5	1.141	9.1	0.963	1.215
	250	20	2.9×10^{-3}	3.253	1.810	3.9	2.157	5.6	0.768	7.5	1.134	9.1	0.958	1.199
	208.5	20	2.7×10^{-3}	3.226	1.33	3.9	2.142	5.6	0.774	7.5	1.130	9.1	0.956	1.191
	100	30	7.3×10^{-4}	3.181	0.87	3.9	2.111	5.8	0.759	7.5	1.126	9.2	0.953	1.165
	0	20	1.6×10^{-3}	3.142	0.53	4.0	2.091	5.8	0.727	7.5	1.124	9.3	0.951	1.148
CHNC II	300	30	7.3×10^{-3}	3.261	−7.50	4.0	2.082	5.6	0.768	7.5	1.120	9.2	0.954	1.212
CHNC I	250	20	6.1×10^{-3}	3.320	4.37	4.0	2.130	5.6	0.792	7.5	1.156	9.2	0.972	1.244
CHNC I	208.5	20	1.8×10^{-3}	3.277	2.78	4.0	2.106	5.6	0.792	7.6	1.144	9.3	0.965	1.218
	100	30	7.0×10^{-3}	3.210	1.52	4.0	2.073	5.8	0.759	7.6	1.134	9.3	0.955	1.182
	0	20	2.7×10^{-3}	3.178	0.81	4.0	2.059	5.8	0.725	7.6	1.133	9.4	0.950	1.145

In this case also we have computed g_k for k_{max} equal to 0.6 from the computed distribution functions for the LJ potential. The PY equation was used for T equal to 210°K and the CHNC equation for $T=183$°K and $T=117$°K. A comparison of these g_k's with the g's for T equal to 210 and 183°K shows that the points belonging to the g_k's follow closely the original g curves. There is no indication of any distortion in the g_k curves, although some of the g_k points lie on one side and others lie on the other side of the g curve. See Figs. 8 and 23. But in the case of $T=117$°K, the g_k curve with k_{max} equal to 0.6, besides being sometimes on one side and sometimes on the other, shows a marked distortion in the first trough of the curve in the neighborhood of 5.8 Å (see Fig. 24). In order to see whether this distortion, and the appreciable difference between g_k with k_{max} equal to 0.6 and the original g, can be reduced by increasing the value of k_{max}, we computed g_k with k_{max} equal to 1.2 Å^{-1}, and found excellent agreement between this g_k and the original g, as can be seen in Fig. 24. From these studies we conclude that the appreciable distortion cannot be introduced into the experimental g's simply because the experimental intensity curves extend at most up to k equal to 0.6 Å^{-1} except for the

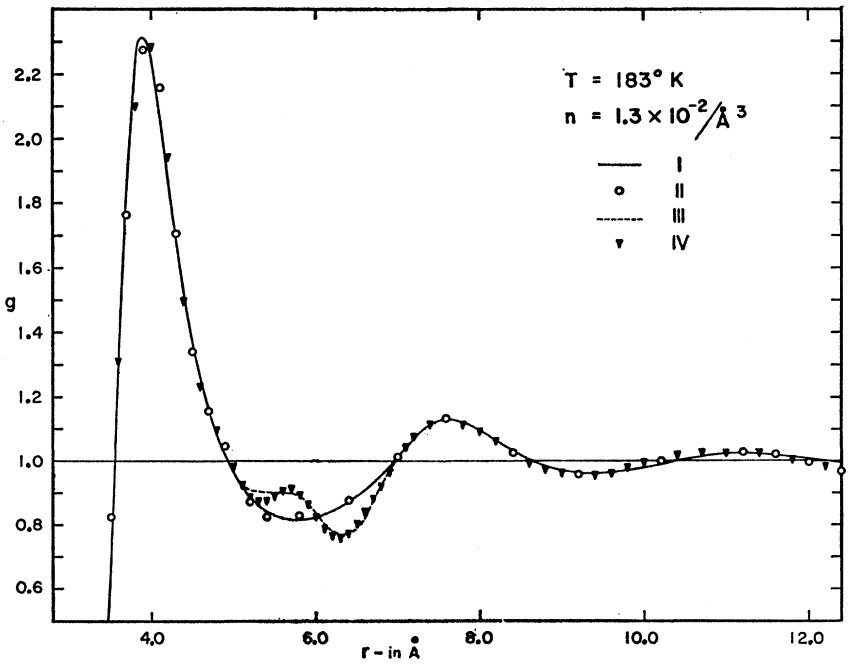

FIG. 23. Curve I is the computed g from the CHNC equation and the LJ potential for the range of integration 20 Å. Curve II is g_k which has been obtained from the curve I first by converting it to intensity curve $i(4\pi k)$ and then reconverting it to the distribution function with the maximum value of $k=0.6$ Å^{-1}. Curve III has been obtained by replacing the part between 5 and 7 Å of curve I by the experimental values of g. Curve IV is the g_k obtained from curve III for the maximum value of $k=0.6$ Å^{-1} in the same way as curve II has been obtained from curve I.

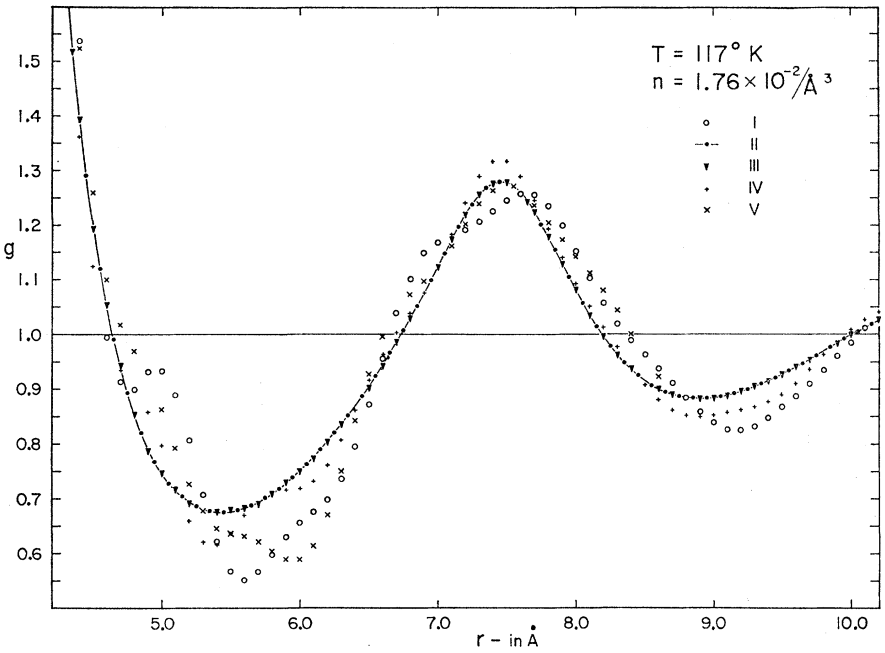

FIG. 24. The curve I is the g computed from the experimental intensity curve without applying any corrections for zero-degree angle scattering. Curve II is the computed LJ-CHNC g for $R=30$ Å. Curve III is the g_k computed from curve II for $k_{\max}=1.2$ Å^{-1}. Curve IV is the g_k computed from curve II for $k_{\max}=0.6$ Å^{-1}. Curve V is the g computed from the experimental intensity curve in which the region between $k=0.46$ and 0.60 Å^{-1} has been replaced by the computed values of intensities from the LJ potential and the CHNC equation.

liquid at very low temperature. The error introduced in the computation of g from i by the equation

$$g_k=1+\frac{8}{nr}\int_0^{k_{\max}} ki(4\pi k)\sin(4\pi kr)dk, \qquad (4.1)$$

due to setting an upper limit on the value of k instead of infinity (called the truncation error) is quite insufficient to account for the distortions present in the experimental g's.

We would like to see which part of the intensity curve must be modified to cause a change in the distribution curve at the place where the distortion in the experimental curve occurs. For this purpose we chose two cases corresponding to the temperatures $T=210$°K and $T=117$°K. At $T=210$°K there are very large irregularities in the experimental distribution function beyond 4.7 Å. The $T=117$°K case has been studied by Clayton and Heaton in detail and has a radial distribution function affected appreciably by the truncation error as has been shown above. First we computed the distribution function g from Eq. (4.1) using the experimental value of $i(s)$. The quantity $i(s)$ is related to the total intensity $I(s)$ by the relation[8]

$$i(s)=[I(s)-I_0]/(I_0-C), \qquad (4.2)$$

where I_0 is a constant intensity at large angles and C is a factor which has been introduced for the purpose of allowing for effects which are independent of angle but cannot be easily calculated.[8] However, we have set $C=0$ in Eq. (4.2) for calculating the value of $i(s)$. The g's computed by us from the experimental values of $i(s)$ were almost the same in form as was obtained by Clayton and Heaton in both cases, but the amplitude of oscillations was magnified in the 210°K temperature case (see Fig. 25). The difference for 117°K case was small. See curve I, Fig. 24.

Since the accurate intensity measurements become more difficult for very small angles because of the presence of the primary beam, and also for large angles because of the small differences between $I(s)$ and I_0, we have studied the effect on the g computed from the $i(s)$ when its values are changed for small values of k and when its values are changed for large values of k. For the 210°K case the computed values of $i(s)$ from the LJ potential and PY equation have been attached to the experimental $i(s)$ curve smoothly at $k=0.11$ Å^{-1} (see Fig. 17). With this hybrid $i(s)$, using theoretical values for $k<0.11$ Å^{-1}, and experimental values for $k>0.11$ Å^{-1}, g was recomputed. The resultant curve is plotted in Fig. 25. The figure shows that the amplitude of oscillations is magnified and the curve as a whole has risen.

In the 117°K case, the experimental $i(s)$ curve was altered for k lying between 0 and 0.1 Å^{-1} by inserting the computed values from the CHNC equation and LJ potential (see Fig. 9). The g was then computed from the new hybrid $i(s)$ and no significant change took place. Next we changed the experimental $i(s)$ for k lying between 0.47 and 0.60 Å^{-1} to the values of i computed from the LJ potential and the CHNC equation (see Fig. 9), and again computed g from this new hybrid $i(s)$. This g is plotted in Fig. 24. A smoothing effect in the g near 4.9 Å (where the maximum irregularity in the experimental curve is present) and near 7.2 Å is very clear. However, there is considerable distortion present in the neighborhood of 5.8 Å. It is interesting to note that there is a marked difference

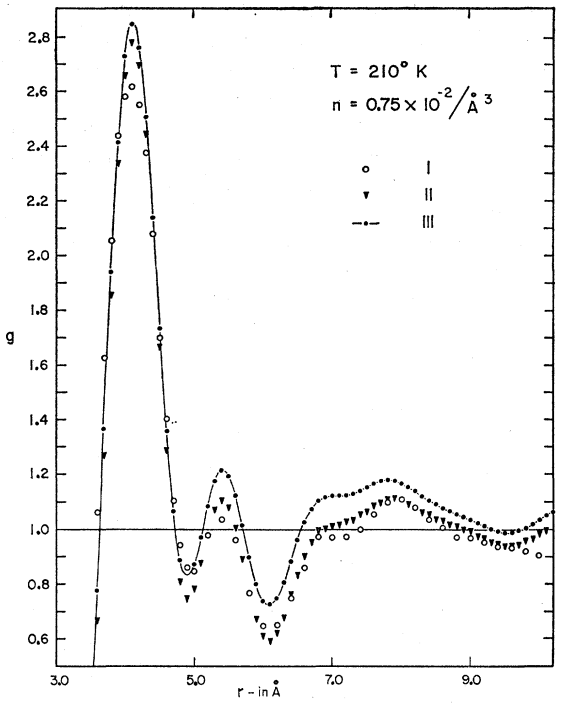

FIG. 25. Curve I is the g as computed by Clayton and Heaton from the experimental intensity curve by using some suitable value of C (see Sec. IV) for the purpose of allowing for effects which are independent of angle. Curve II is the g computed by us from the experimental intensity curve by putting $C=0$. Curve III is the g computed from the intensity curve which is obtained by joining the computed (LJ-PY) intensity curve to the experimental curve at $k=0.11$ Å^{-1}. The computed intensity curve extends from $k=0$ Å^{-1} to $k=0.11$ Å^{-1} and the experimental intensity curve extends from $k=0.11$ Å^{-1} to $k=0.6$ Å^{-1}. The joining has been done smoothly.

between the computed and the experimental values of $i(s)$ for k lying between 0.47 and 0.6 Å (the difference is not only in the magnitude, but also the experimental maxima is shifted towards left), and it is near 5.8 Å that the distortion due to truncation error is at a maximum (as discussed before). A marked shift towards the left of the fourth experimental maxima relative to the fourth maxima of the computed $i(s)$ curves is prominent for the 117, 133, and 153°K cases. The shapes of the irregularities and their locations in the g curves of these cases are also very much alike, as can be seen in Figs. 2, 4, and 19.

From the above considerations it follows that the truncation error causes some irregularities in the distribution function of liquids at low temperatures, yet it cannot be the major cause. The major cause of the irregularities in the distribution functions is inherent in the experimentally measured intensity curves.

In Fig. 26 we have plotted the intensity curves at 183°K computed from the LJ-CHNC g (curve I, Fig. 23). We have also shown the intensity curve which has been computed from the LJ-CHNC g modified in the region lying between 5 and 7 Å by replacing it by the experimental values of g (curve III of Fig. 23). The difference between these two intensity curves (curves 1 and 2 of Fig. 26) is small. The differences are of an order which can be accounted for by the experimental errors. However, both these curves differ very much from the experimental intensity curve. (The experimental distribution function is not in agreement with the computed g's in the location of the first peak, as can be seen from the Fig. 6.) The difference is probably too great to be entirely due to experimental error. It can be accounted for partly by the differences in the experimental and the computed g's in the regions other than that lying between 5 and 7 Å (particularly in the region of the first peak), and partly by errors in measurements. But if we take into consideration the fact that the irregularity in the experimental g appears rather markedly in the neighborhood of 5 Å in the cases of 117, 133, 153, and 183°K, and near the second maxima in the cases of 117, 133, and 153°K, it seems rather unlikely that this is due entirely to experimental error. It appears that the irregularities in the experimental distribution functions are due to the presence of structure in the liquid.

The computed g's from the integral equations using the LJ and GM potentials are smooth curves. It may be that equating Z to a constant value instead of a

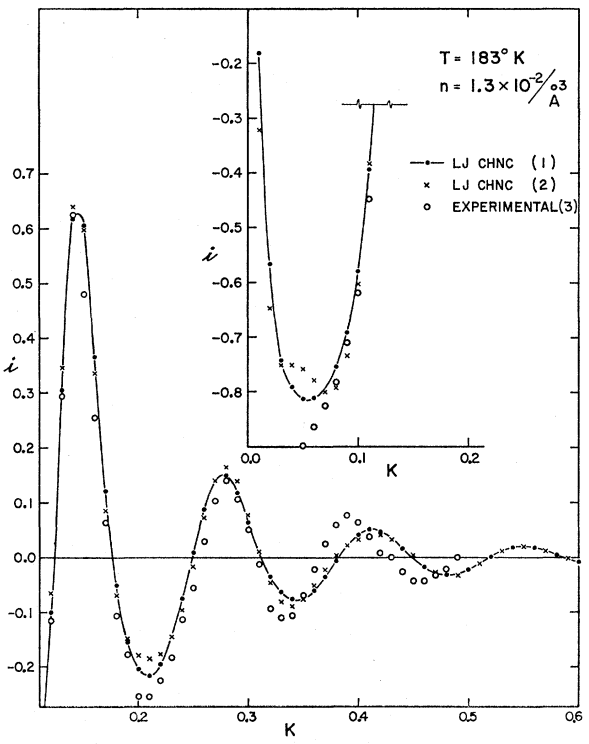

FIG. 26. Curve I is the computed intensity curve at $T=183$°K with the LJ potential and CHNC equation. Curve III is the experimental intensity curve and curve II is the intensity curve computed from the LJ–CHNC g which has been modified by replacing the part between 5 and 7 Å by the experimental g.

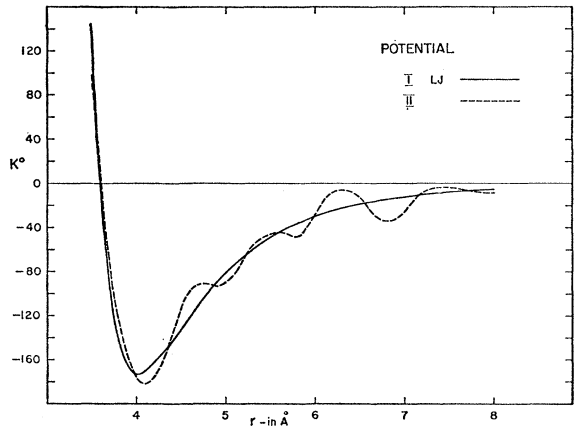

FIG. 27. Curve I is the LJ potential for krypton. Curve II is the potential function which is expected to introduce irregularities in the computed distribution functions of the type present in the experimental g's.

function of distance gives a smooth distribution function when a smooth potential is used. The only way to introduce irregularities in the computed g's like the irregularities in the experimental g's is to introduce irregularities in the potential function. Curve II of Fig. 27 shows an approximate form of the pair interaction which would introduce the type of irregularities present in the experimental g's into the computed g's. Curve II has been computed from the CHNC integral equation using the experimental diffraction data. The details of the method of solving the equation for the potential are given elsewhere.[36]

V. CONCLUSIONS

From the discussions of the integral equations in Sec. II and the results of computations and their comparisons in Sec. III and the study of the experimental distribution functions, we have been able to derive the following conclusions:

(1) A suitable value of Z depending on the temperature and the density would give a better g than is obtained by $Z=0$ or $Z=-1$.

(2) The g's computed using the LJ (6-12) potential with the constants due to Beattie *et al.* and the CHNC equation are in good agreement with the experimental curves at temperatures close to the critical temperature.

(3) The experimental distribution curve near the critical temperature (210°K) gives too high a first peak. The computed curve is probably more reliable than the experimental curve.

(4) The computed g's are not affected appreciably by a change in the range of integration for solving the integral equations provided it is greater than 20 Å. The compressibilities are affected very strongly by a change in the range of integration. The longer the range, the higher the computed compressibility. The range of integration after which the compressibility will not be affected appreciably is rather too large to be practically feasible for solving the integral equations numerically.

(5) The effect on the computed g's of changing the long-range part of the pair potential is small. The first peak rises with an increase in the value of λ/k. We could not find the CHNC case-I kind of solution when the value of λ/k was increased to 300°K.

(6) The major cause of the irregularities in the experimental distribution functions is inherent in the experimentally measured intensity curves and not the truncation error.

(7) There is very strong indication by the experimental g's that the irregularities in the experimental g's are due to the actual presence of structure in the liquid.

ACKNOWLEDGMENTS

The author wishes to thank Professor A. A. Broyles for many discussions and suggestions, Dr. B. S. Thomas for a discussion on Fourier transform techniques, R. A. Smith for the computer programming, and G. Scheffer for drawing the graphs. The author is indebted to the staff of the University of Florida Computing Center for making available their IBM 709 computer.

APPENDIX

The Lennard-Jones and the Guggenheim-McGlashan potentials for krypton are given below.

(i) The LJ potential is given by

$$\phi=4\epsilon[(a/r)^{12}-(a/r)^{6}], \tag{A1}$$

where the constants used are[11]

$$\epsilon/k=172.70°\mathrm{K},$$
$$a=3.591\ \text{Å}.$$

The value of r where the potential energy is minimum is r_0 given by

$$r_0=4.030\ \text{Å}.$$

(ii) The GM potential is given by

$$\phi(r)=\infty, \quad r<d, \tag{A2}$$

$$\phi(r)=-\epsilon+K\frac{(r-r_0)^2}{r_0^2}-\alpha\frac{(r-r_0)^3}{r_0^3}\frac{(2r_0-r)}{r_0}, \tag{A3}$$

$$r_1\leqq r\leqq r_2,$$

$$\phi(r)=-\lambda(r_0/r)^6, \quad r\leqq r_3. \tag{A4}$$

[36] A. A. Khan (to be published).

The constants are

$$\epsilon/k=191.1°\text{K};\quad K/k=62.4\times10^2\ °\text{K},$$
$$\alpha/k=27.2\times10^3\ °\text{K};\quad r_0=4.077\ \text{Å},$$
$$\lambda/k=208.5°\text{K};$$
$$d=3.4\ \text{Å};\quad r_1=3.8\ \text{Å},$$
$$r_2=4.4\ \text{Å};\quad r_3=5.8\ \text{Å}.$$

The derivatives of the GM potential used in these computations are given below.

$$d\phi/dr=0,\quad r\leqq3.3\ \text{Å}.$$

$d\phi/dr$ is given in the tabular form (Table IV) for r lying between 3.4 and 5.8 Å,

$$\frac{d\phi}{dr}=\frac{1251\times(4.077)^6}{r^7},\quad r\geqq5.8\ \text{Å}.$$

TABLE IV. The potential function ϕ and its derivatives between 3.3 and 5.7 Å.

r	ϕ(°K)	ϕ'	r(Å)	ϕ(°K)	ϕ'
3.3	∞	0	4.6	−138.47	119.65
3.4	0	−382.00	4.7	−125.00	128.33
3.5	−37.00	−382.00	4.8	−112.00	128.33
3.6	−75.00	−382.00	4.9	−99.00	128.33
3.7	−114.00	−382.00	5.0	−86.00	128.33
3.8	−153.18	−308.74	5.1	−73.00	128.33
3.9	−177.02	−172.82	5.2	−61.00	103.00
4.0	−188.69	−65.13	5.3	−51.00	98.00
4.1	−190.91	16.64	5.4	−43.00	79.00
4.2	−186.14	74.87	5.5	−39.00	59.11
4.3	−176.64	111.92	5.6	−31.50	44.61
4.4	−164.39	130.16	5.7	−27.80	33.33
4.5	−151.16	131.95			

Table IV gives the potential function ϕ and its derivatives between 3.3 and 5.8 Å.